Electronic Supplementary Material (ESI) for New Journal of Chemistry.

Supporting Information

Synthesis and structure-properties correlation of blue fluorescence isomer emitters based on rigid pyrazine-bridged carbazole frameworks

Lingjuan Wei, Jie Li, Kai Xue, Shanghui Ye and Hongji Jiang *

(Nanjing University of Posts and Telecommunications, Institute of Advanced Materials, Key Laboratory for Organic Electronics and Information Displays and Jiangsu Key Laboratory for Biosensors, Jiangsu National Synergetic Innovation Center for Advanced Materials, Nanjing 210023)

Table S1. Data results of linear fitting of the Lippert–Magada equation for the compounds **TCz-3PA-TCz**, **TCz-3,9PA-TCz** and **TCz-9PA-TCz**

	$\lambda_{abs,\ max}$ (nm)				[a] $\lambda_{em,\ max}$ (nm)				Intercept	slope	[b] R^2	[c] a(Å)	μ_{ge}(D)
	toluene	$CHCl_3$	EA	THF	toluene	$CHCl_3$	EA	THF					
TCz-3PA-TCz	392	396	390	391	424	453	431	433	1926.92	2829.34	0.84	7.19	1.02
TCz-3,9PA-TCz	388	400	389	390	431	464	438	440	2576.85	1718.55	0.78	7.19	0.80
TCz-9PA-TCz	391	404	391	390	451	482	458	458	3393.85	1966.82	0.90	7.19	0.85

[a] Excitation wavelength =315 nm. [b] R^2 represents a linear correlation coefficient. [c] a is the onsagar cavity radius

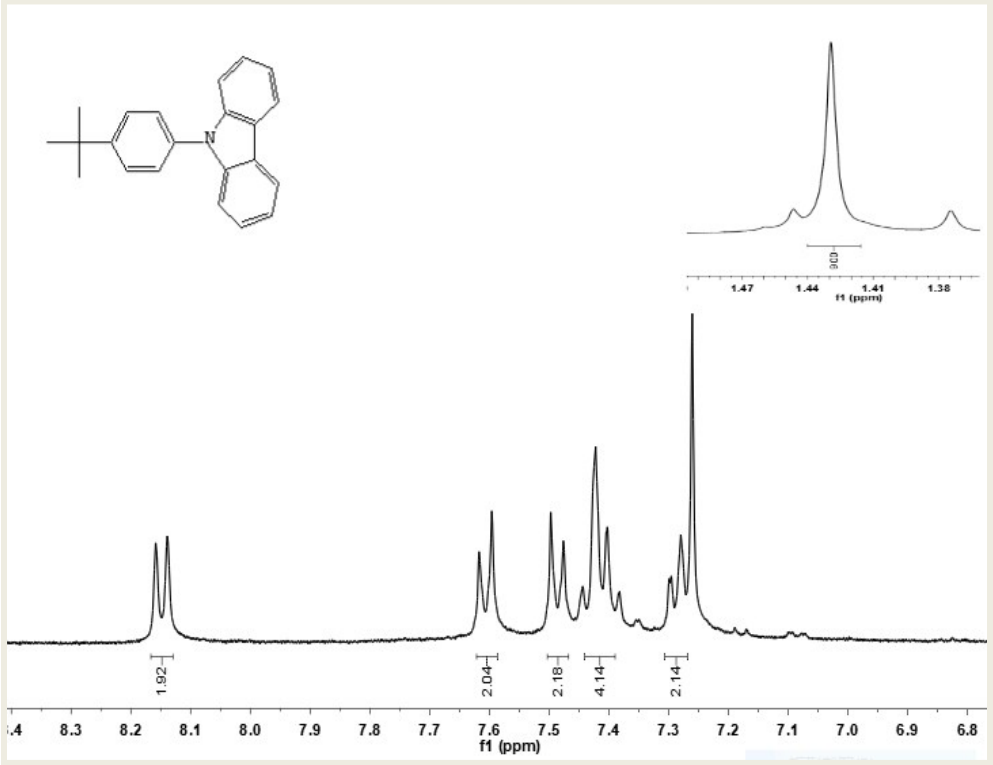

Figure S1. The ^{1}H-NMR spectrum of **9-(4-(tert-butyl)phenyl)-9H-carbazole** ($CDCl_3$, 400 MHz, ppm)

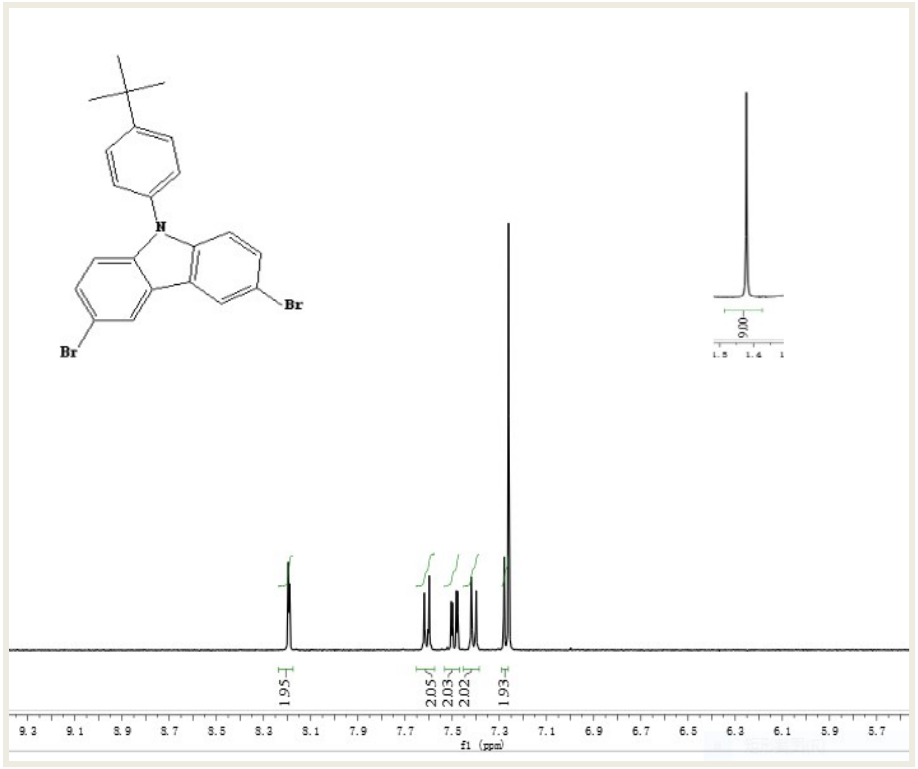

Figure S2. The ^{1}H-NMR spectrum of **3,6-dibromo-9-(4-(tert-butyl)phenyl)-9H-carbazole** ($CDCl_3$, 400 MHz, ppm)

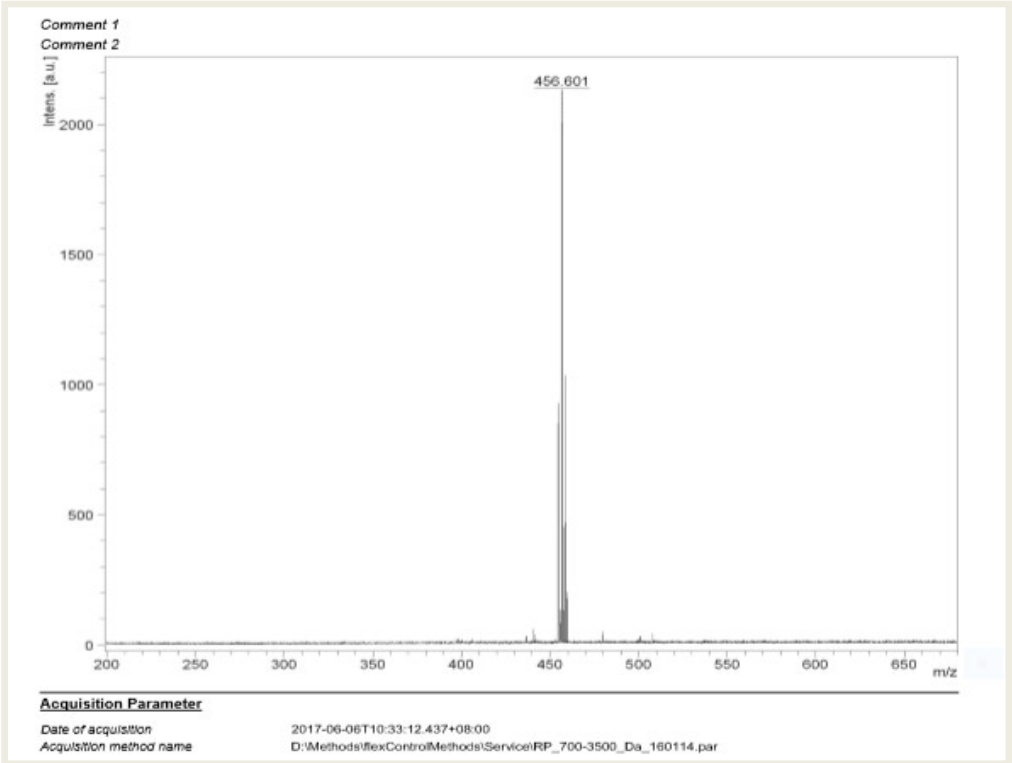

Figure S3. The MALDI-TOF spectrum of **3,6-dibromo-9-(4-(tert-butyl)phenyl)-9H-carbazole**

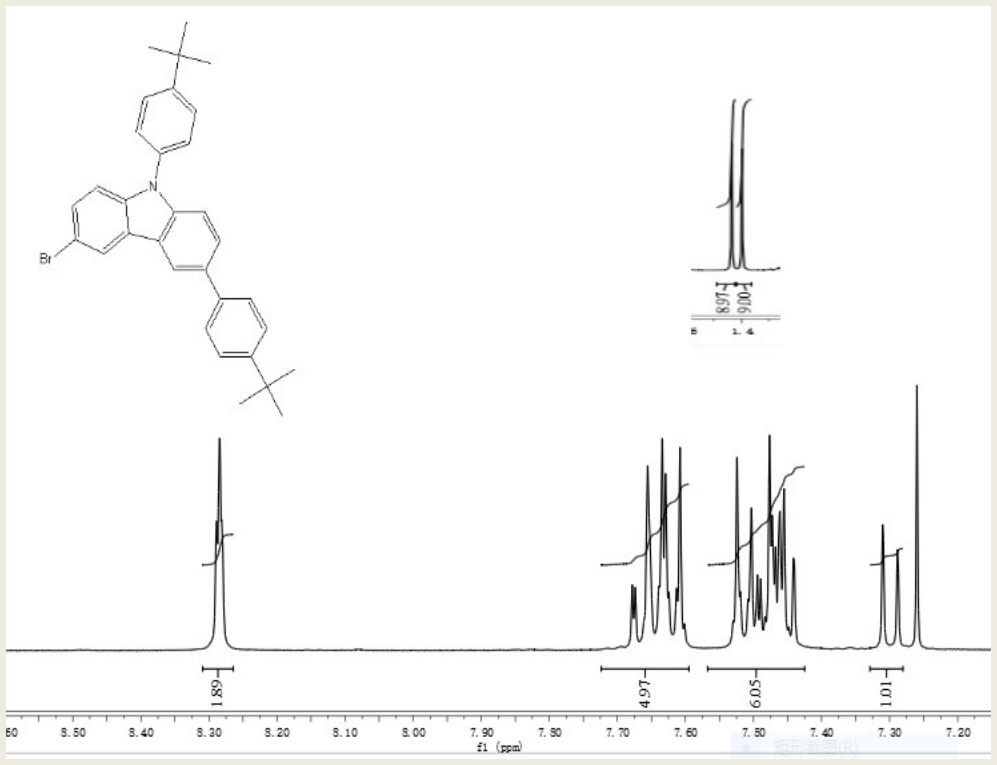

Figure S4. The ^{1}H-NMR spectrum of **3-bromo-6,9-bis(4-(tert-butyl)phenyl)-9H-carbazole** ($CDCl_3$, 400 MHz, ppm)

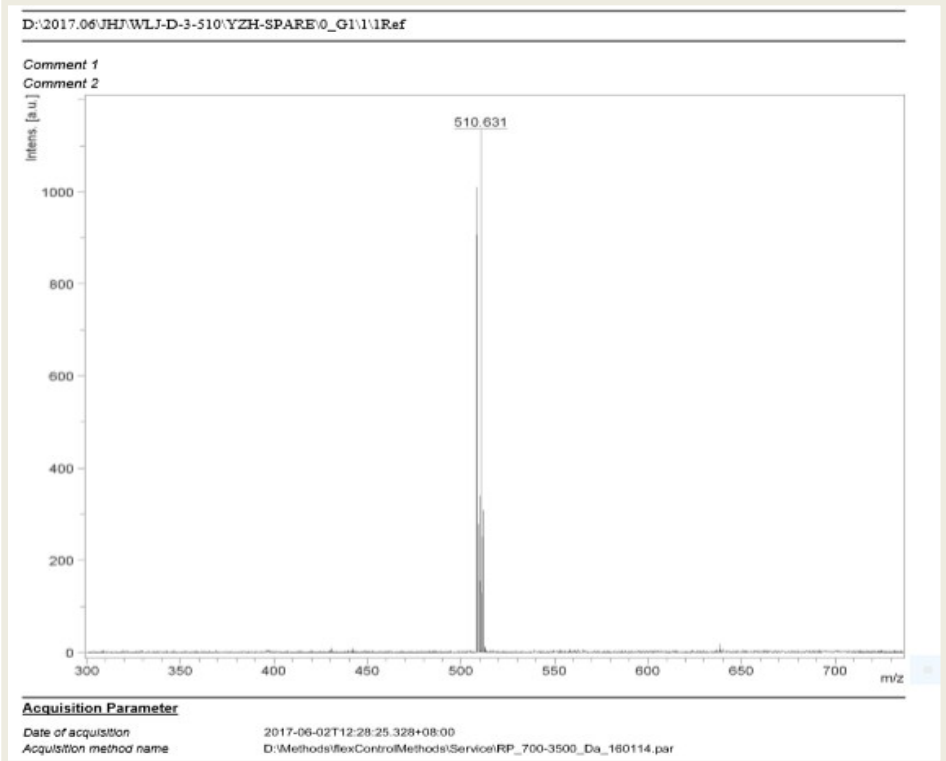

Figure S5. The MALDI-TOF spectrum of **3-bromo-6,9-bis(4-(tert-butyl)phenyl)-9H-carbazole**

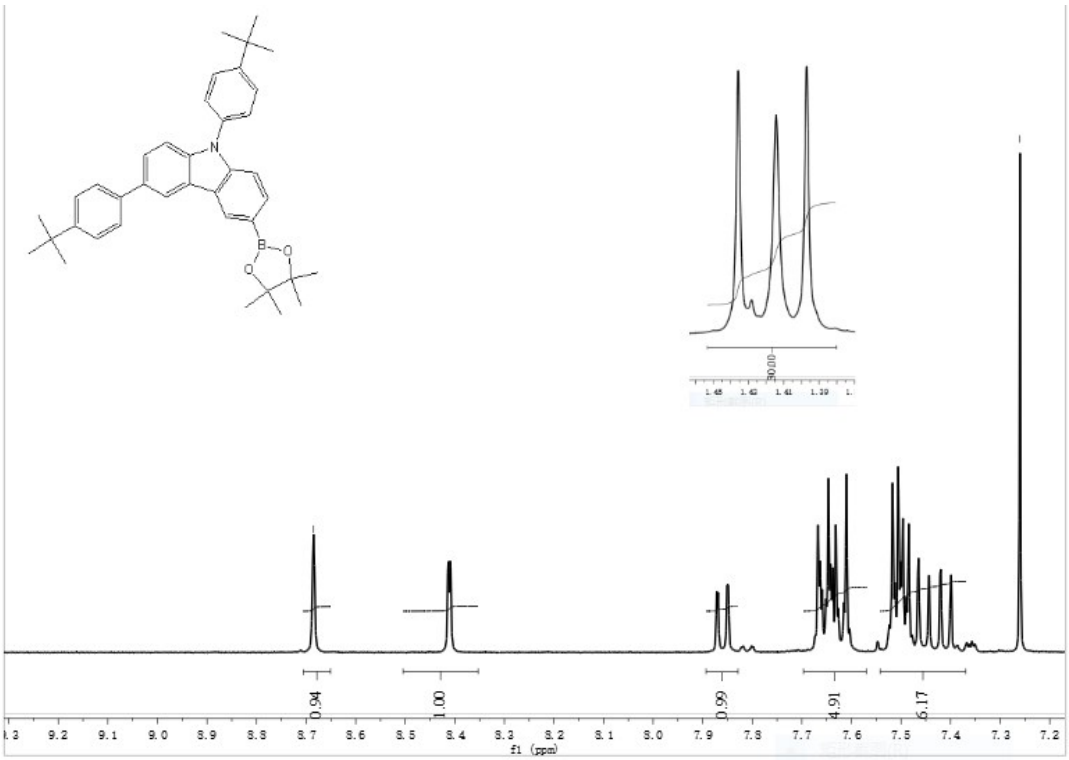

Figure S6. The ^{1}H-NMR spectrum of **3,9-bis(4-(tert-butyl)phenyl)-6-(4,4,5,5-tetramethyl-1,3,2-dioxaborolan-2-yl)-9H-carbazole** ($CDCl_3$, 400 MHz, ppm)

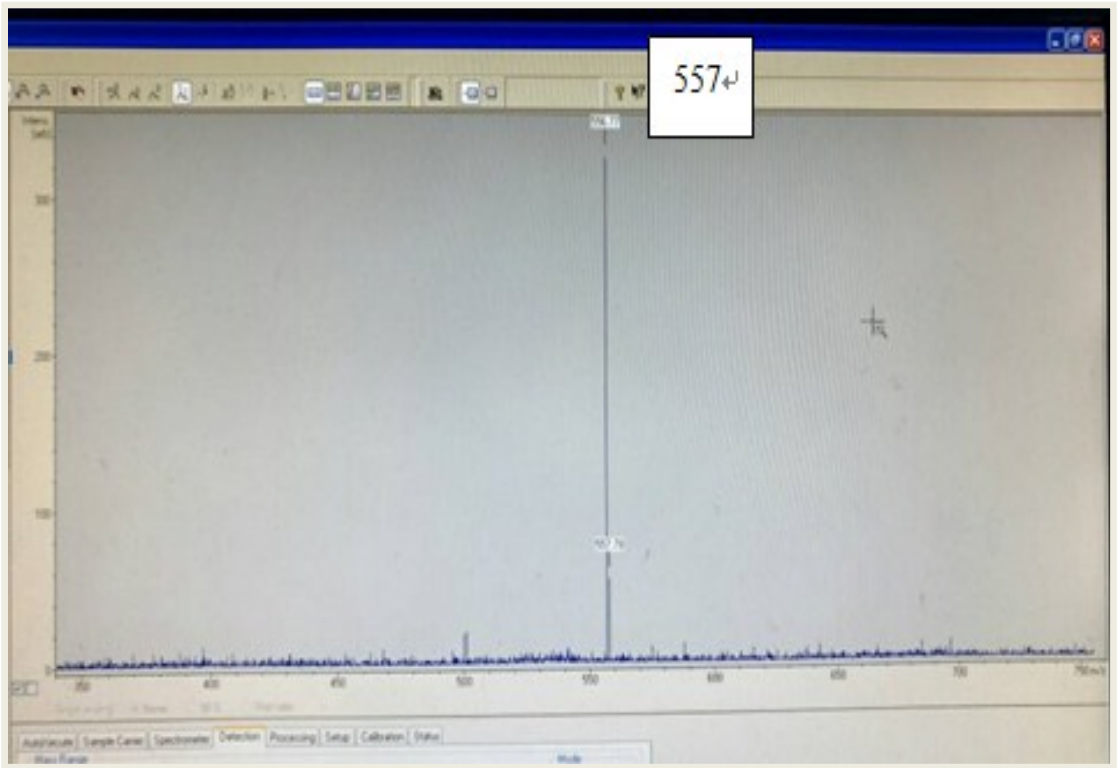

Figure S7. The MALDI-TOF spectrum of **3,9-bis(4-(tert-butyl)phenyl)-6-(4,4,5,5-tetramethyl-1,3,2-dioxaborolan-2-yl)-9H-carbazole**

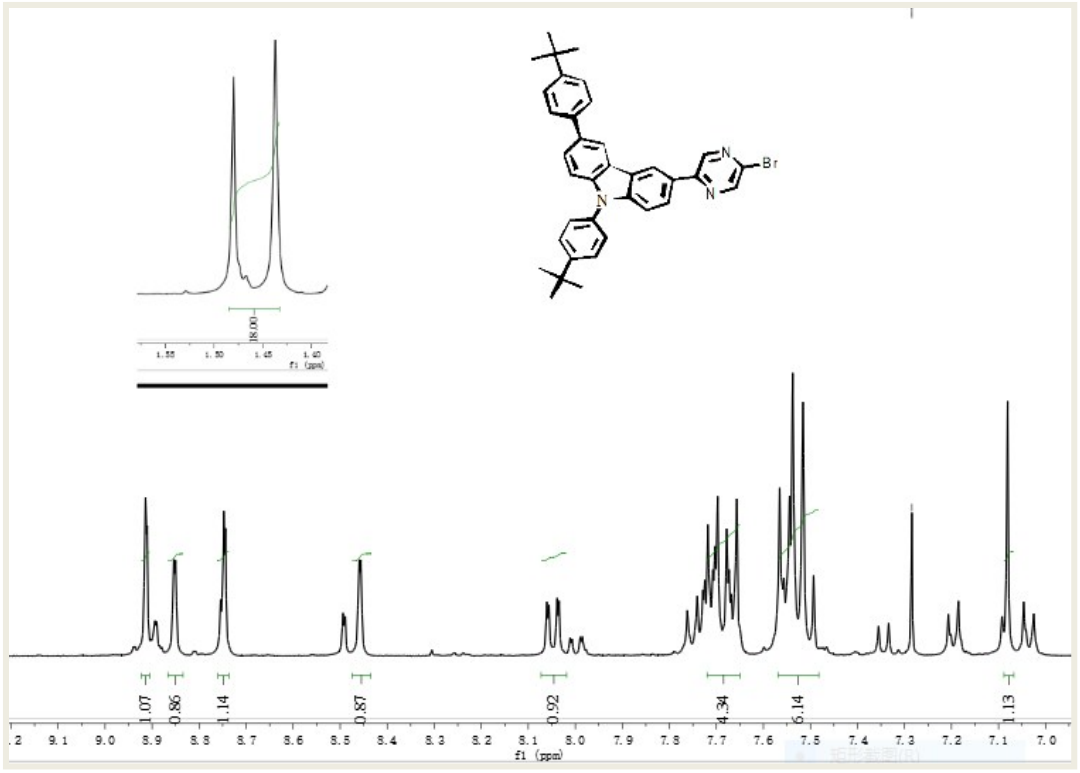

Figure S8. The ^{1}H-NMR spectrum of **L1** ($CDCl_3$, 400 MHz, ppm)

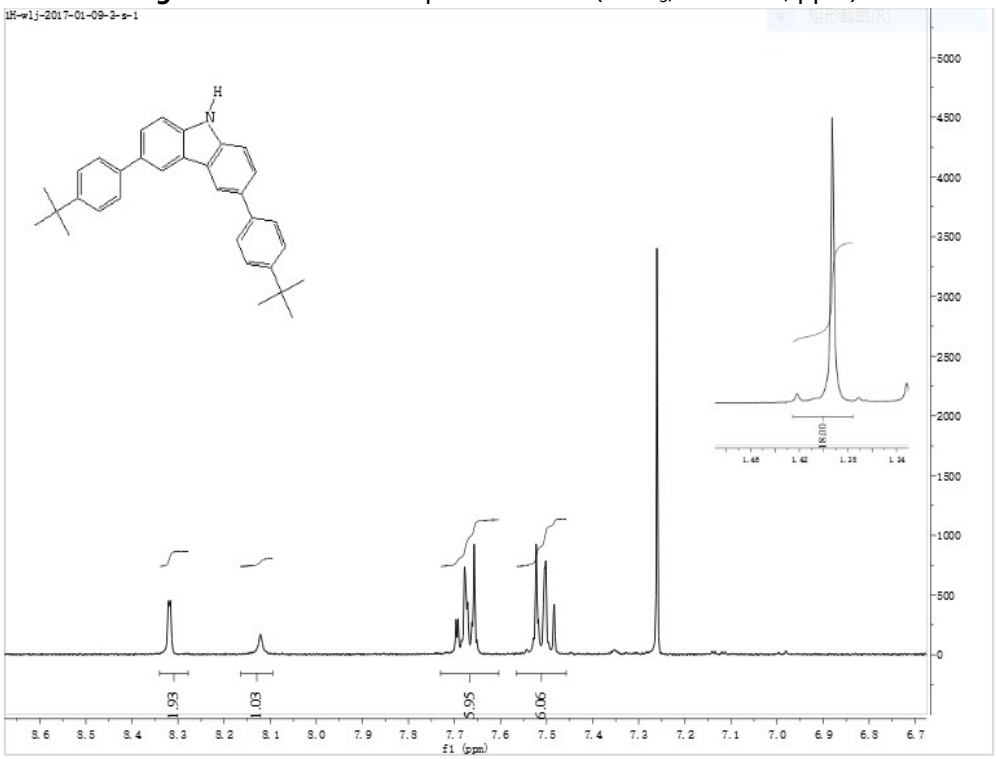

Figure S9. The ^{1}H-NMR spectrum of **3,6-bis(4-(tert-butyl)phenyl)-9H-carbazole** ($CDCl_3$, 400 MHz, ppm)

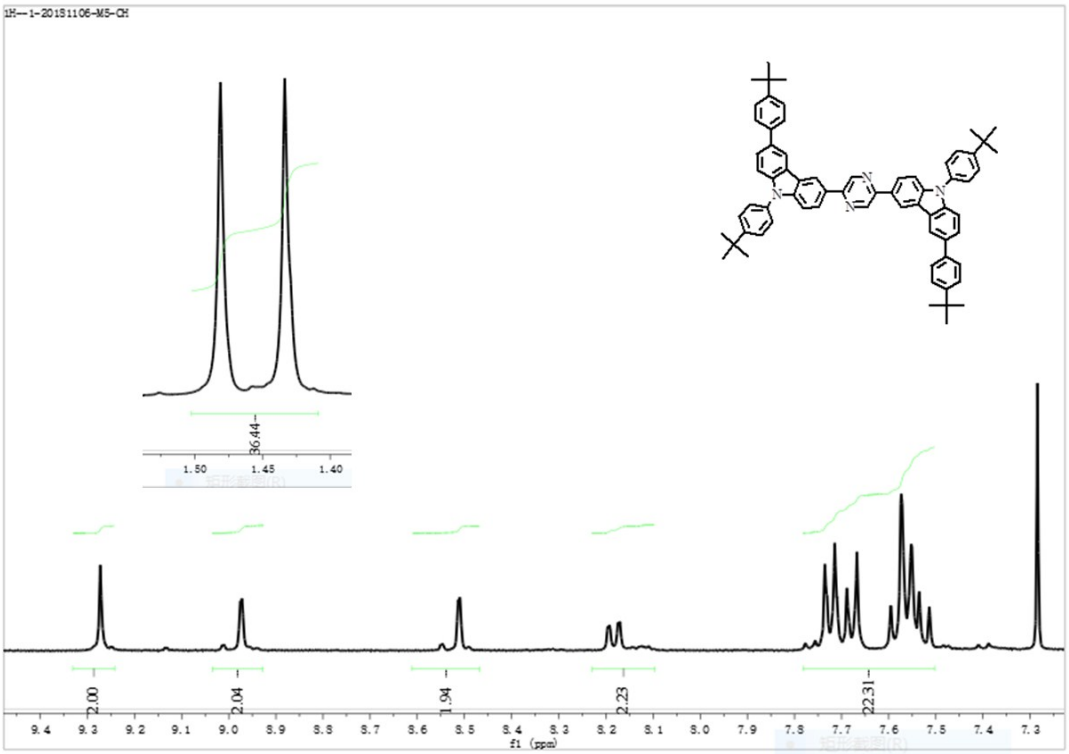

Figure S10. The ^{1}H-NMR spectrum of **TCz-3PA-TCz** ($CDCl_3$, 400 MHz, ppm)

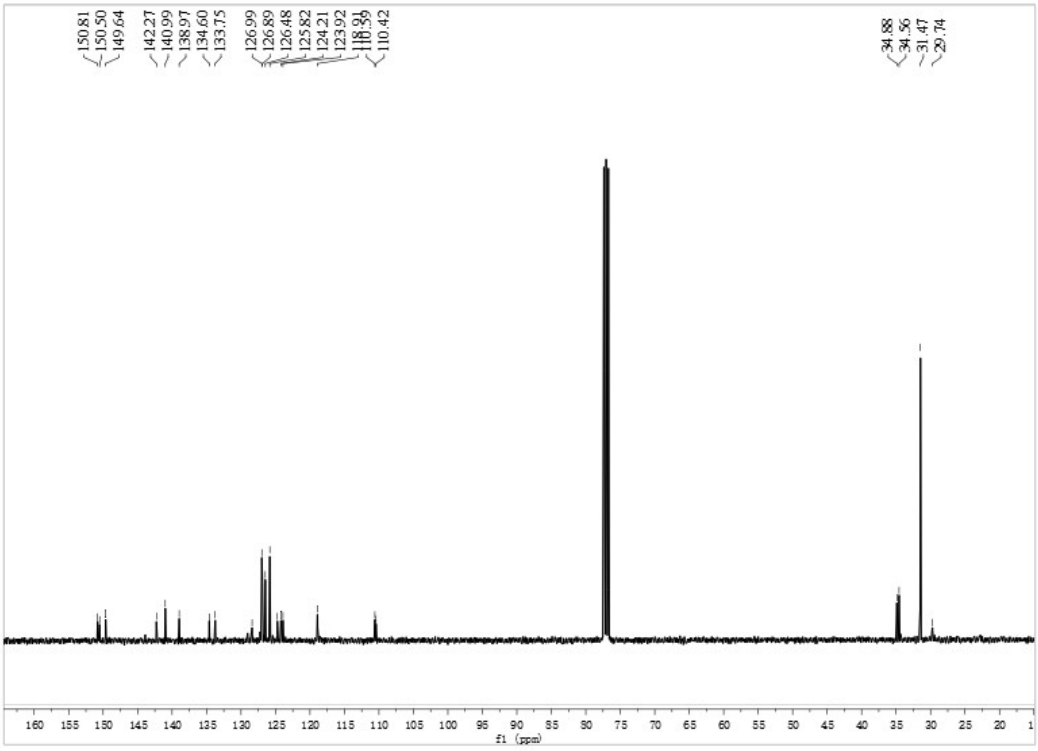

Figure S11. The ^{13}C-NMR spectrum of **TCz-3PA-TCz** ($CDCl_3$, 100 MHz, ppm)

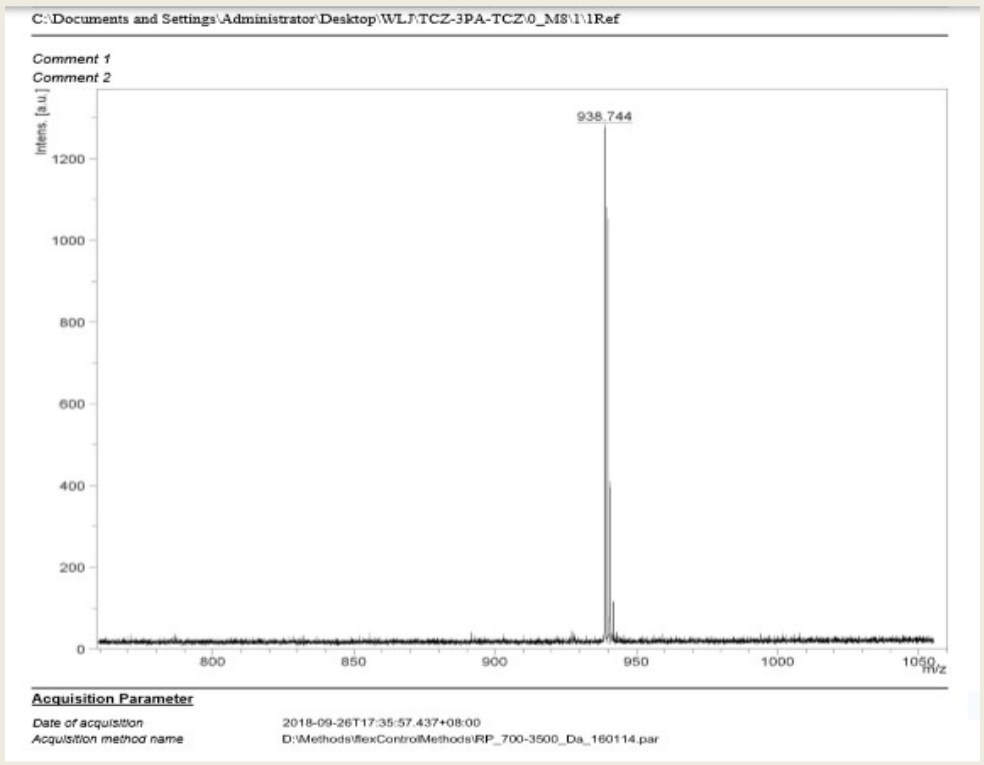

Figure S12. The MADI-TOF spectrum of **TCz-3PA-TCz**

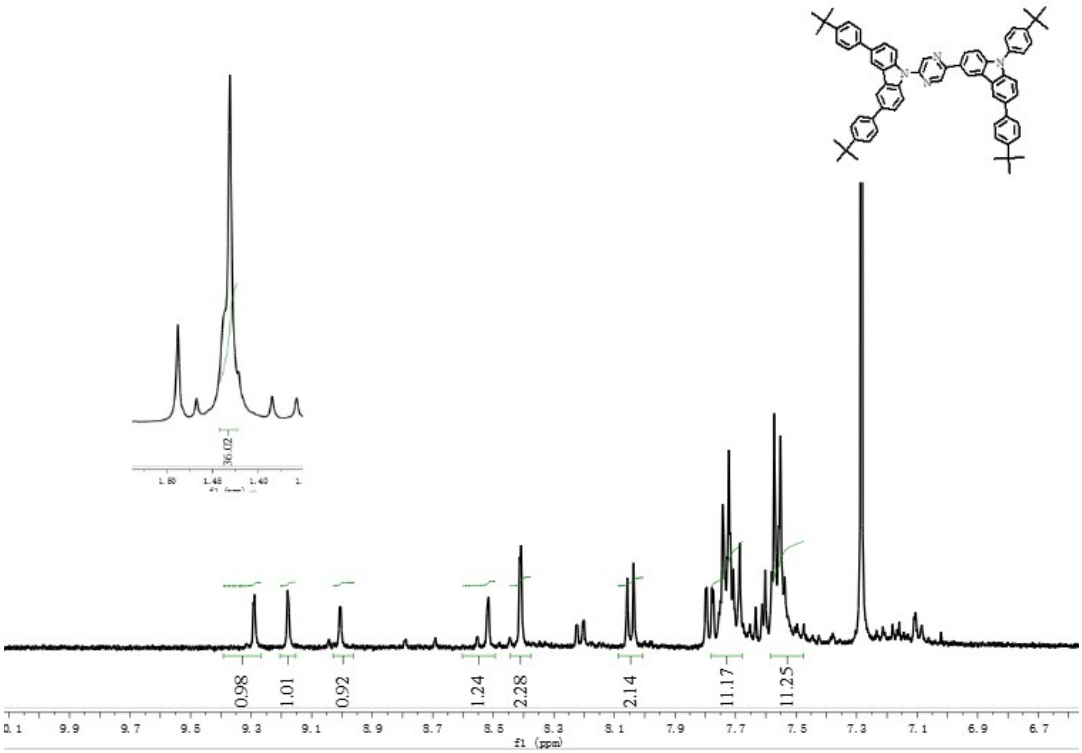

Figure S13. The ^{1}H-NMR spectrum of **TCz-3,9PA-TCz** ($CDCl_3$, 400 MHz, ppm)

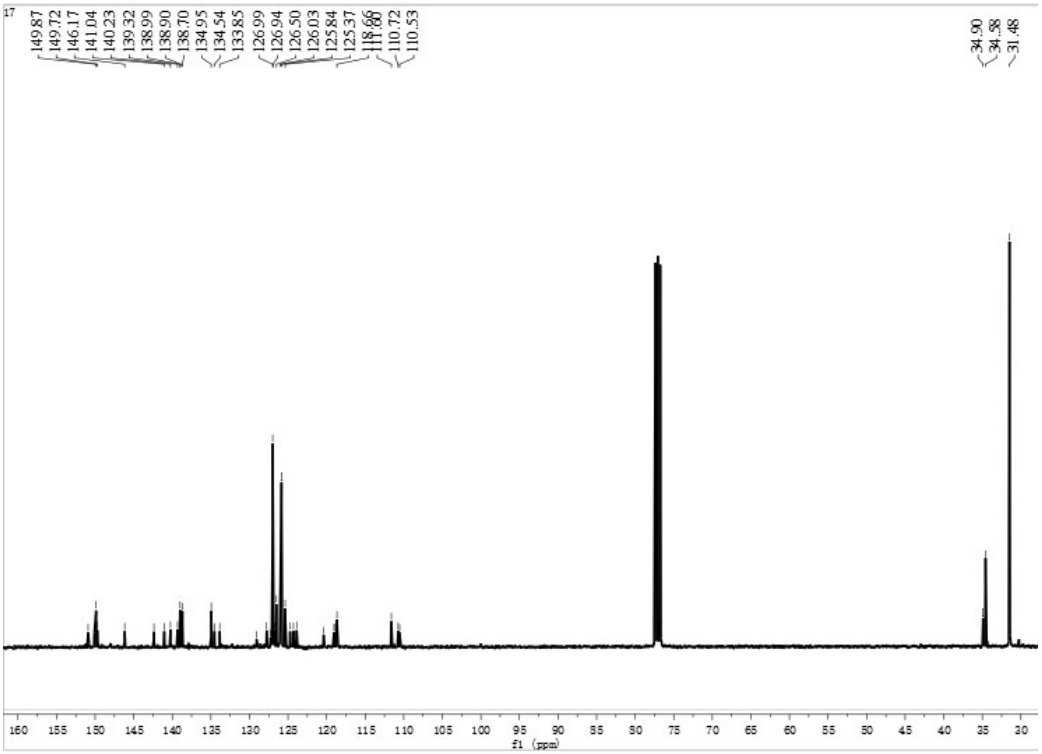

Figure S14. The ^{13}C-NMR spectrum of **TCz-3,9PA-TCz** ($CDCl_3$, 100 MHz, ppm)

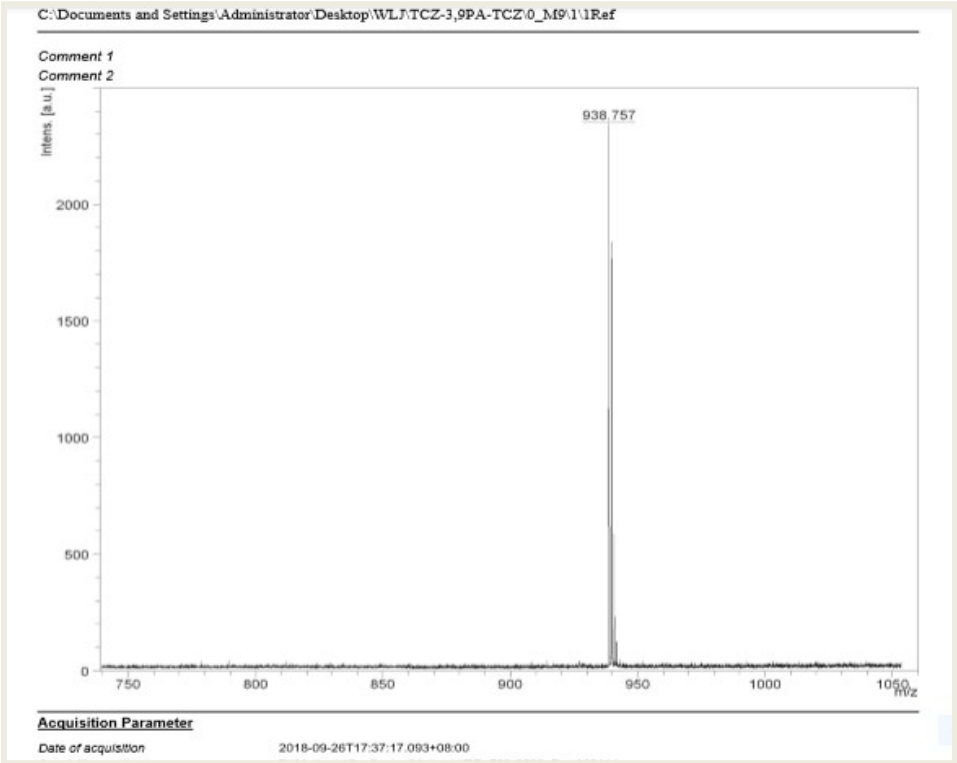

Figure S15. The MALDI-TOF spectrum of **TCz-3,9PA-TCz**

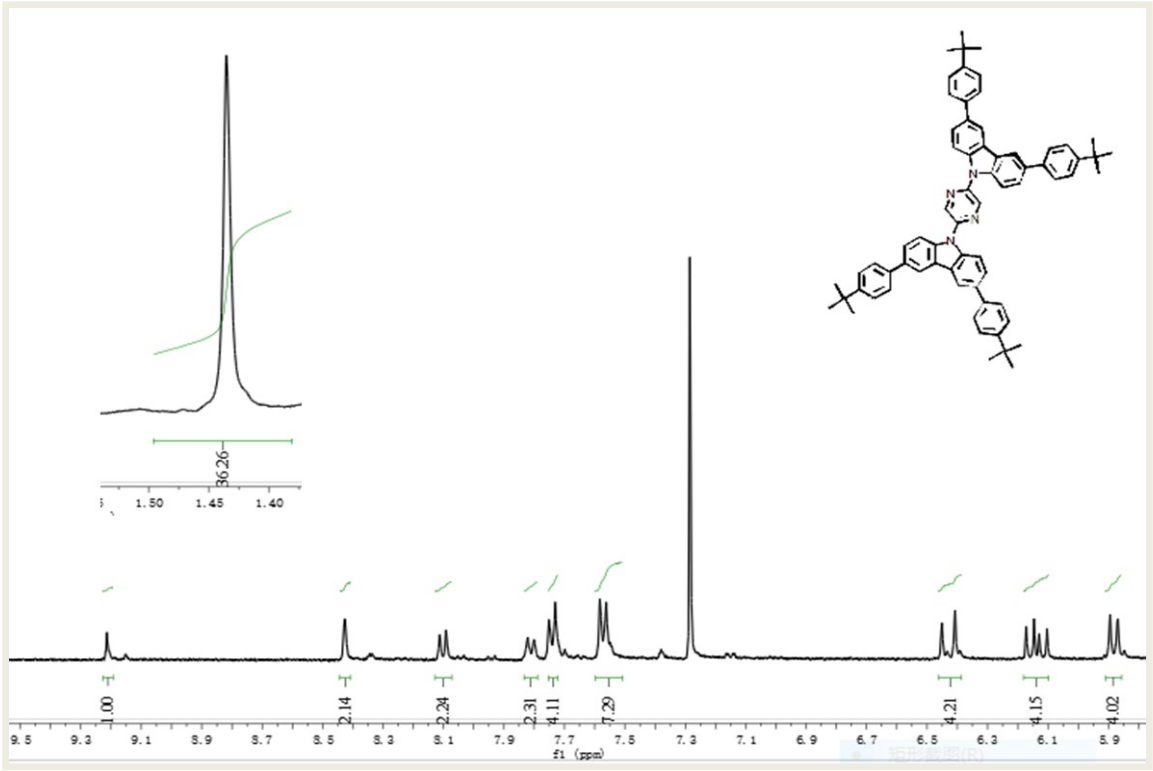

Figure S16. The ^{1}H-NMR spectrum of **TCz-9PA-TCz** ($CDCl_3$, 400 MHz, ppm)

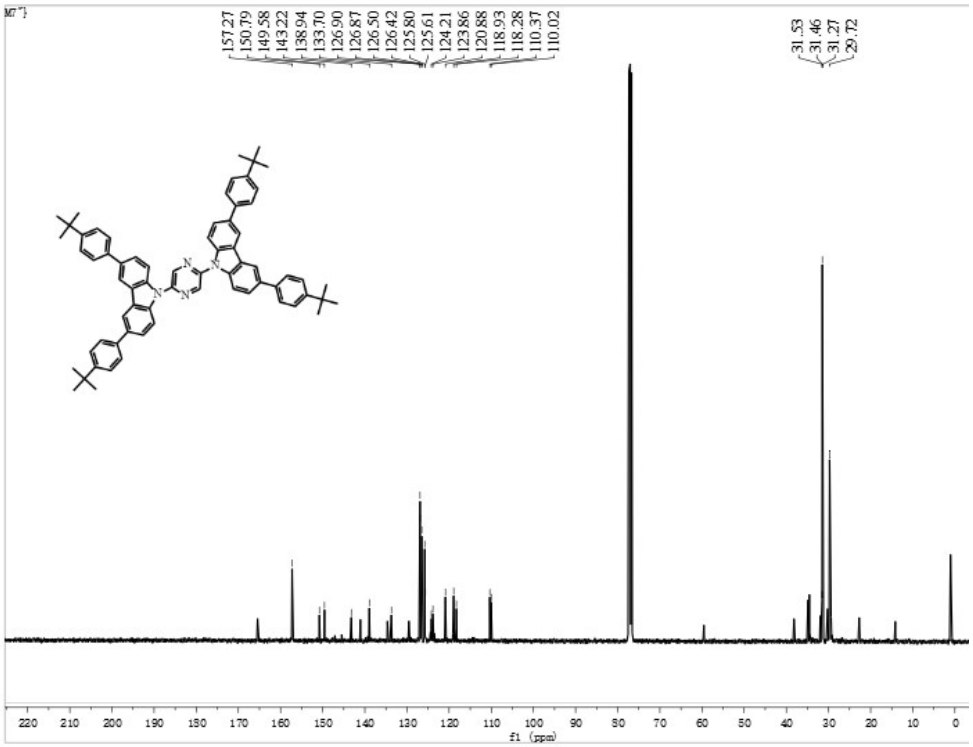

Figure S17. The ^{13}C-NMR spectrum of **TCz-9PA-TCz** ($CDCl_3$, 100 MHz, ppm)

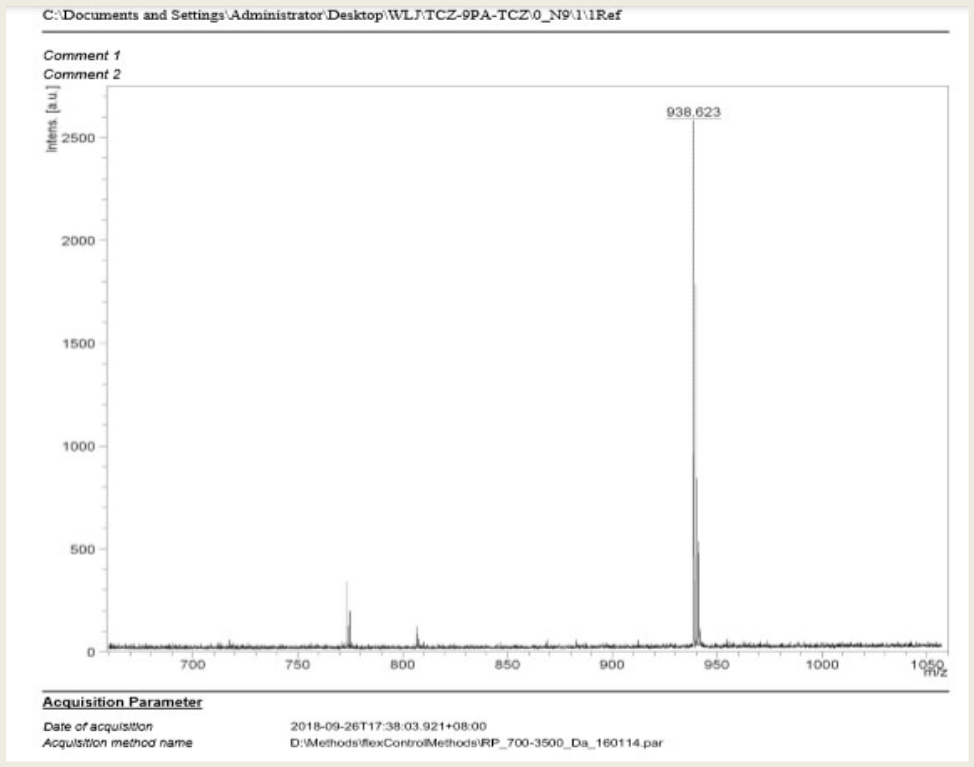

Figure S18. The MALDI-TOF spectrum of **TCz-9PA-TCz**

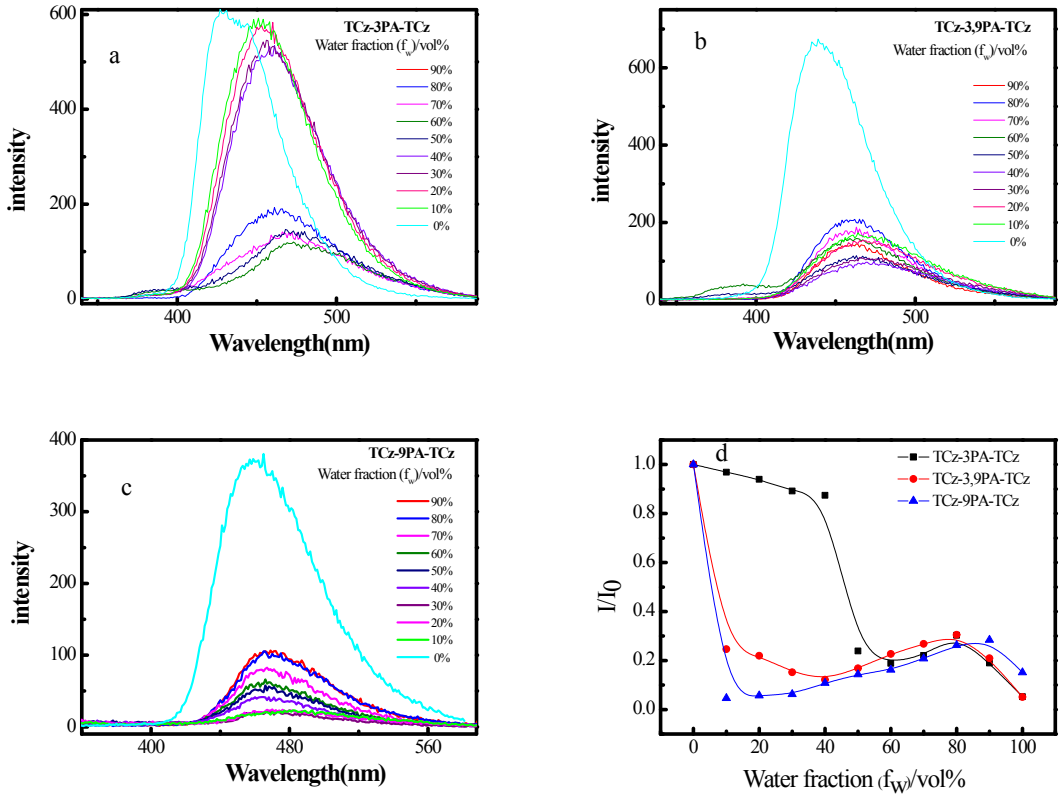

Figure S19. The PL emission spectra of compounds **TCz-3PA-TCz** (a), **TCz-3,9PA-TCz** (b) and **TCz-9PA-TCz**

(c) in the tetrahydrofuran and water mixtures with different water fractions (f_w) at a fixed concentration of 1 × 10^{-5} mol/L. The plot of relative PL emission intensity (I/I_0) versus f_w (I and I_0 are PL emission intensity in the mixture and pure tetrahydrofuran solution(d)

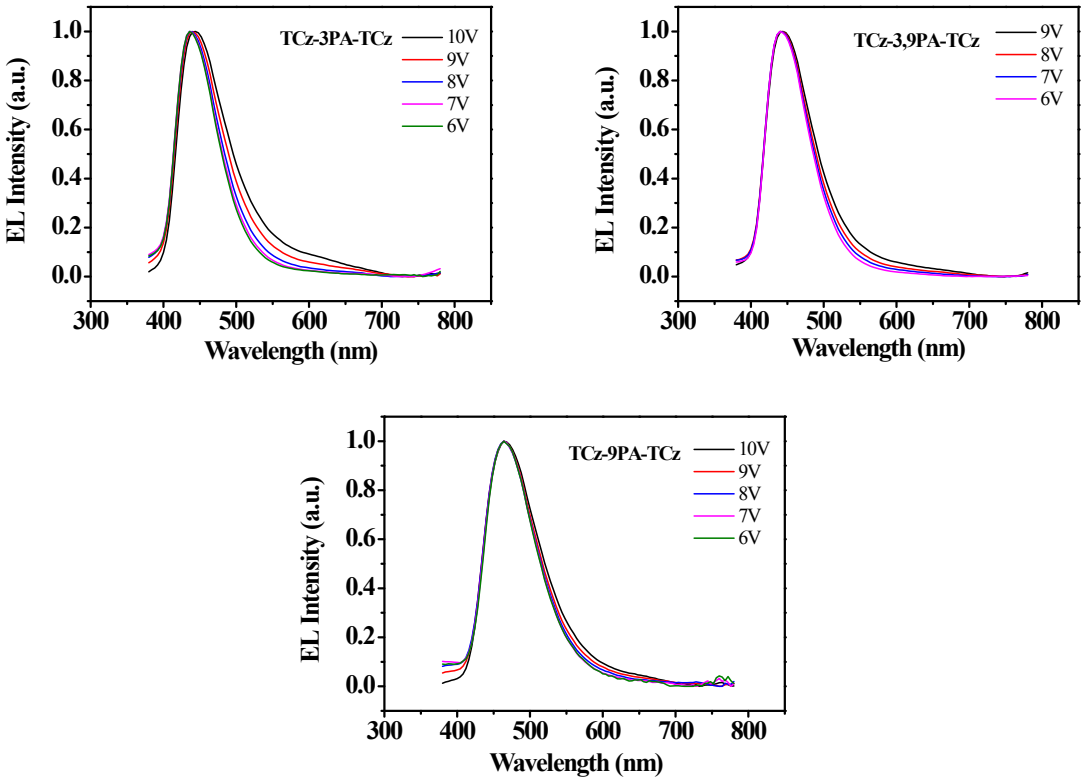

Figure S20. The electroluminescent spectra of devices based on **TCz-3PA-TCz**, **TCz-3,9PA-TCz** and **TCz-9PA-TCz** by solution spin coating.

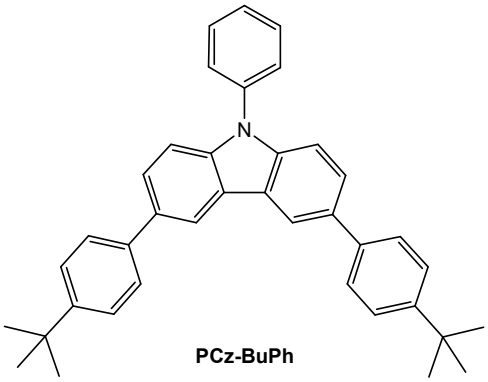

PCz-BuPh

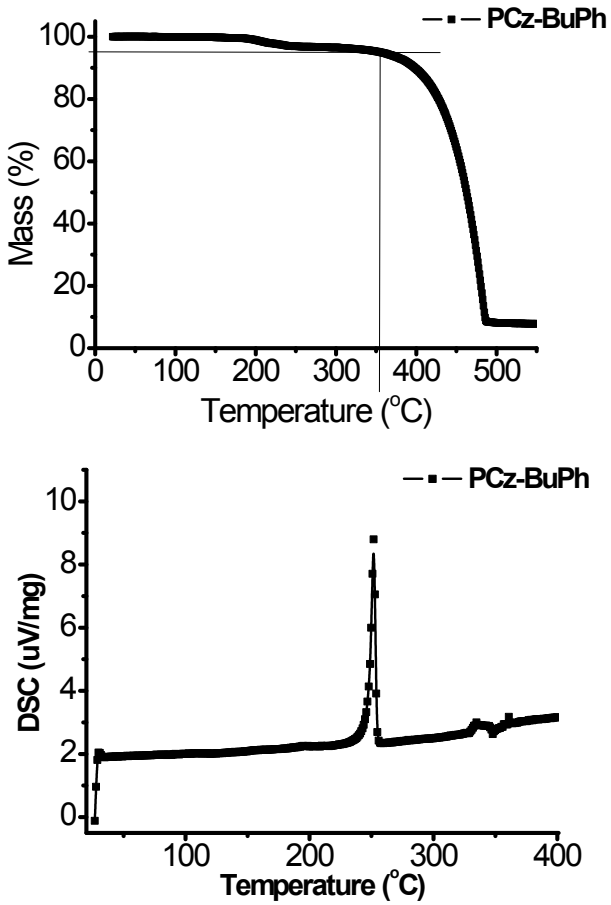

Figure S21. The TGA and DSC curves of emitter **3,6-Bis-(4-*tert*-butyl-phenyl)-9-phenyl-9H-carbazole (PCz-BuPh)** in the solid powder state

OLED devices performance based on **PCz-BuPh** fabricated by solution spin coating method

Device structure: ITO/PEDOT:PSS (30 nm) /CBP:pvk:OXD-7:15% **PCz-BuPh**(55 nm) /TPBi(35 nm)/Ca:Ag,

CIEx,y /V	11	10	9	8	7	6
x	0.2238	0.2066	0.1933	0.1852	0.1801	0.1772
y	0.2044	0.1678	0.1402	0.1245	0.1157	0.1136

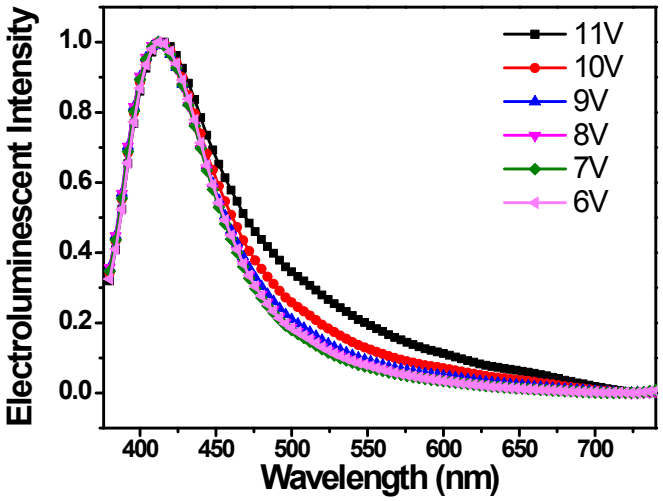

Figure S22. The electroluminescent spectra of the device based on **PCz-BuPh**

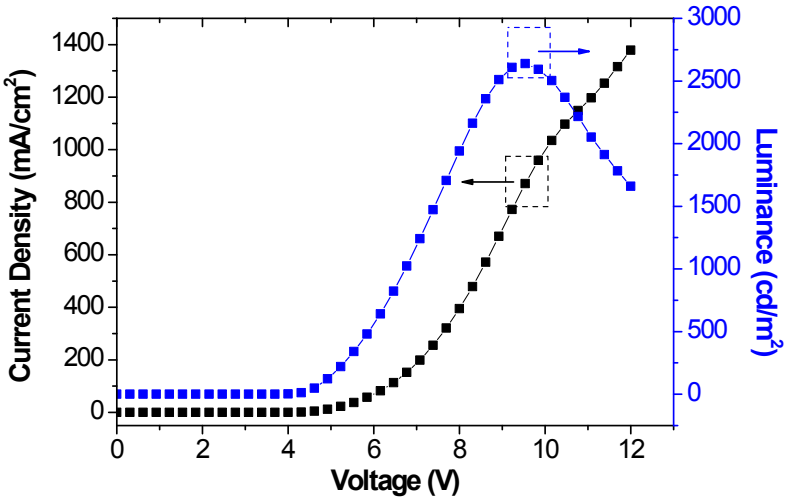

Figure S23. Current density-voltage-luminance characteristics of the device based on **PCz-BuPh**

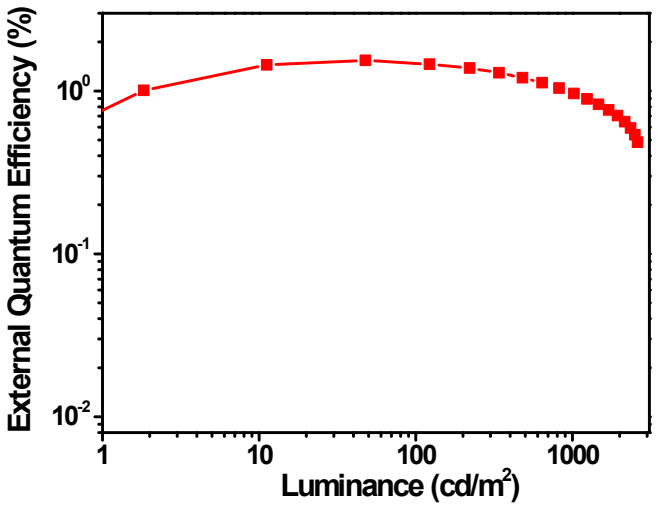

Figure S24. The external quantum efficiency-luminance characteristics of the device based on **PCz-BuPh**

OLED devices performance based on **PCz-BuPh** fabricated by thermal deposition in vacuum

Device structure:

(1) ITO/MoO_3(1 nm)/TAPC (20 nm)/mCP(10 nm)/DPEPO: **PCz-BuPh** (30%, 25nm)/TmPyPB (40 nm)/LiF (0.7 nm)/Al(120nm)

(2)ITO/MoO_3(1 nm)/TAPC (20 nm)/mCP(10 nm)/DPEPO: **PCz-BuPh** (20%, 25nm)/TmPyPB (40 nm)/LiF (0.7 nm)/Al(120nm)

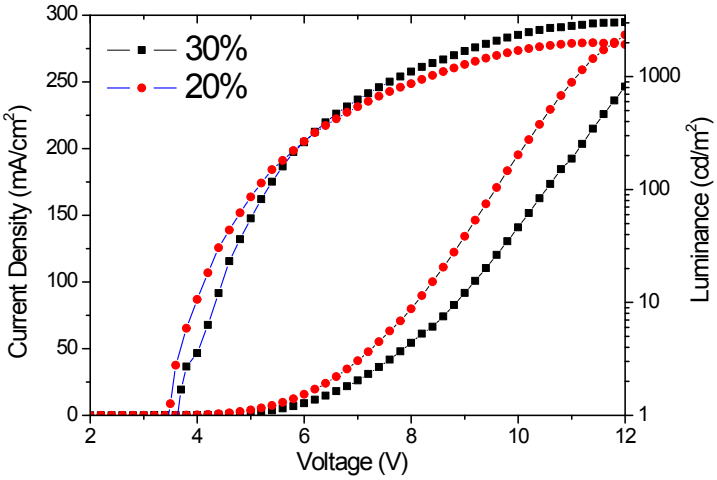
30%
20%
Current Density (mA/cm^2)
Luminance (cd/m^2)
Voltage (V)
0
50
100
150
200
250
300
1
10
100
1000
2
4
6
8
10
12

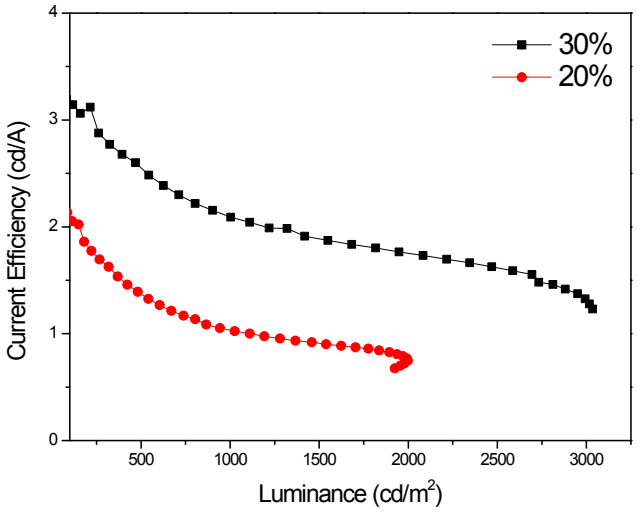
30%
20%
Current Efficiency (cd/A)
Luminance (cd/m^2)
0
1
2
3
4
500
1000
1500
2000
2500
3000

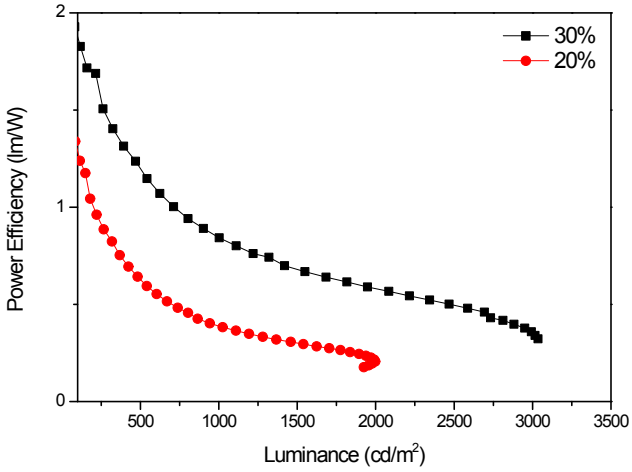
30%
20%
Power Efficiency (lm/W)
Luminance (cd/m^2)
0
1
2
500
1000
1500
2000
2500
3000
3500

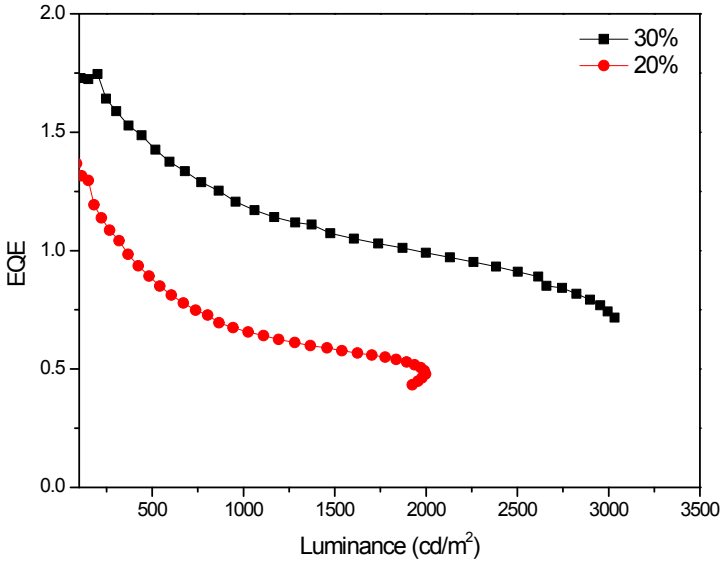

Devices	V_{on} (V)	λ_{ems} (nm)	PE_{max} (lm/w)	CE_{max} (cd/A)	100cd/m^2		1000cd/m^2		EQE @100 cd/m^2
					PE (lm/w)	CE (cd/A)	PE (lm/w)	CE (cd/A)	
30%	3.7	398	1.82	3.14	1.82	3.14	0.84	2.09	1.72
20%	3.5	399	1.23	2.05	1.23	2.05	0.38	1.02	1.31

Figure S25. Current density−voltage−luminance characteristics, current efficiency-luminance characteristics, power efficiency-luminance characteristics, the external quantum efficiency-luminance characteristics of the devices and summary of blue OLED performance of the devices **PCz-BuPh** fabricated by thermal deposition in vacuum